ResearchGate

See discussions, stats, and author profiles for this publication at: https://www.researchgate.net/publication/44653668

Structure, Morphology, and Bioactivity of Biocompatible Systems Derived from Functionalized Acrylic Polymers Based on 5-Amino-2-naphthalene Sulfonic Acid

ARTICLE *in* BIOMACROMOLECULES · JULY 2010

Impact Factor: 5.75 · DOI: 10.1021/bm100223d · Source: PubMed

CITATIONS
9

READS
33

7 AUTHORS, INCLUDING:

Luis García-Fernández
Spanish National Research Council
25 PUBLICATIONS **106** CITATIONS
SEE PROFILE

Maria Rosa Aguilar
Spanish National Research Council
70 PUBLICATIONS **617** CITATIONS
SEE PROFILE

Mar Fernandez Gutierrez
Spanish National Research Council
81 PUBLICATIONS **641** CITATIONS
SEE PROFILE

Rosa M Lozano
Centro de Investigaciones Biológicas
51 PUBLICATIONS **1,178** CITATIONS
SEE PROFILE

Available from: Mar Fernandez Gutierrez
Retrieved on: 02 February 2016

Structure, Morphology, and Bioactivity of Biocompatible Systems Derived from Functionalized Acrylic Polymers Based on 5-Amino-2-naphthalene Sulfonic Acid

L. García-Fernández,[†,‡] M. R. Aguilar,[*,†,‡] M. M. Fernández,[§] R. M. Lozano,[||] G. Giménez,[||] S. Valverde,[⊥] and J. San Román[†,‡]

Biomaterials Department, Institute of Polymer Science and Technology (ICTP, CSIC), Juan de la Cierva 3, 28006 Madrid, Spain, Networking Biomedical Research Centre in Bioengineering, Biomaterials and Nanomedicine, CIBER-BBN, Spain, Pharmacology Department, Faculty of Pharmacy, Universidad Complutense de Madrid (UCM), Ciudad Universitaria s/n, 28040 Madrid, Spain, Department of Chemical and Physical Biology, Centre for Biological Research (CIB, CSIC), Ramiro de Maeztu 9, 28040 Madrid, Spain, and Department of Bioorganic Chemistry, Organic Chemistry Institute (IQO, CSIC), Juan de la Cierva 3, 28006 Madrid, Spain

Received March 1, 2010; Revised Manuscript Received April 9, 2010

New therapeutic strategies for the treatment of neoplastic pathologies and, in particular, metastasis processes are based on the inhibitory effect of angiogenic processes. The present article deals with the design, preparation, and application of new "polymer drugs" with a clear inhibitory effect of the activation of fibroblast growth factors, which plays an important role in the proliferation of vascular cells and, consequently, in tumor angiogenesis. Two different copolymer systems based on 5-methacrylamide-2-naphthalenesulfonic acid (MANSA) and butylacrylate (BA) or vinylpyrrolidone (VP) were prepared by free radical copolymerization and exhaustively characterized. The molecular weight of the copolymers was moderate but both families presented very homogeneous macromolecular populations with a polydispersity index very close to unity, which indicates that MANSA presents a noticeable effect on the polymerization processes. The system poly(BA-*co*-MANSA) provides amphiphilic copolymers that give rise to the formation of oriented micelles with a core of the hydrophobic BA segments and a shell of MANSA components. The average size of these self-assembling nanoparticles is between 20 and 100 nm, depending on the composition of the copolymer system. However, poly(VP-*co*-MANSA) systems are more hydrophilic and give more homogeneous and water-soluble macromolecules. The bioactivity of both systems was studied by the analysis of proliferation of Balb/c 3T3 fibroblasts in the presence of acidic fibroblast growth factor (aFGF) as a function of the concentration of poly(BA-*co*-MANSA) or poly(VP-*co*-MANSA), and the results obtained demonstrated that the MANSA-containing polymers were not toxic for cells, but induced a clear inhibition of cell proliferation in the presence of aFGF. The effect was polymer-concentration dependent, but the activity was noticeably higher for poly(BA-*co*-MANSA) copolymers, owing to the self-assembled micellar morphology of the nanoparticles, which placed the sulfonic groups in the more adequate position to interact with the growth factor. These systems offer a good alternative for low toxicity treatments of angiogenic, processed based on inhibition of the activity of growth factors.

Introduction

Antiangiogenic therapy is one of the main strategies in the treatment of certain diseases in which the formation of blood vessels is upregulated, such as cancer, diabetes blindness, and psoriasis. A wide range of neoplastic pathologies have been treated with therapies based on the application of antiangiogenic agents. The inhibition of endothelial cell proliferation in tumors and, consequently, the modulation of blood vessels neoformation, inhibits tumor growth, decreases tumor mass, and induced tumor regression.[1−4] This kind of therapy presents several advantages if compared to the therapy directed against tumor cells because it targets activated endothelial cells. Specially, activated endothelial cells are easily accessible by systemic administration as they are directly in contact with blood. Moreover, different tumor cells are sustained by a single capillary, and consequently, inhibition of a small number of tumor vessels may affect the growth of many tumor cells.

Proliferation of activated endothelial cells can be inhibited by different means, for example, blocking the angiogenesis promoting factors, such as fibroblast growth factors (FGFs). This family of pro-angiogenic polypeptides plays a very important role in the proliferation, migration, and differentiation of vascular cells and also plays a decisive role in tumor angiogenesis.[5] FGF needs to interact with different kinds of receptors (FGFRs) to be active, that is, the transmembrane signaling receptors with intrinsic tyrosine kinase activity and a family of cell surface heparin sulfate proteoglycans (HSPG). It has been reported that the interaction of FGF with these cell surface heparinlike molecules produce the FGF oligomerization, which is necessary for FGF to recognize their specific tyrosine kinase receptor. The former are responsible for the biological response, but the later are required for the FGFRs to be active.

* To whom correspondence should be addressed. Tel.: +34915618806 (ext. 212). Fax: +34915644853. E-mail: mraguilar@ictp.csic.es.
[†] ICTP, CSIC.
[‡] Networking Biomedical Research Centre in Bioengineering.
[§] UCM.
[||] CIB, CSIC.
[⊥] IQO, CSIC.

10.1021/bm100223d © 2010 American Chemical Society
Published on Web 06/08/2010

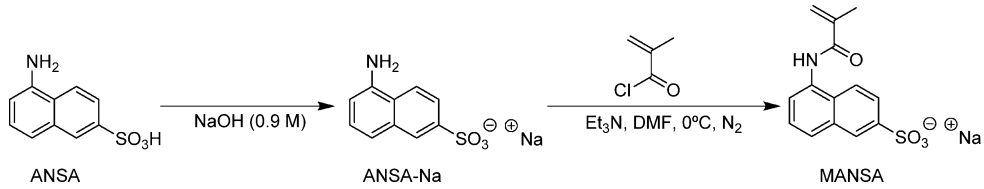

Figure 1. Synthesis of methacrylic derivative of ANSA.

Table 1. Composition and Molecular Weight of the Synthesized Poly(BA-*co*-MANSA) Obtained by ^{1}H NMR and GPC

	composition				GPC		
	$F(BA)_{feed}$	$f(BA)_{copol}$	$w(BA)_{copol}$	yield (%)	M_w	M_n	M_w/M_n
poly(BA-*co*-MANSA) (30:70)	30	80	64	35.2	17000	12200	1.40
poly(BA-*co*-MANSA) (60:40)	60	82	67	29.1	20400	18600	1.10
poly(BA-*co*-MANSA) (70:30)	70	89	78	31.3	40300	18500	2.18

Some of the most promising family of molecules with this effect are suramin and suradistas families.[6,7] In this way, naphthalene sulfonate family constitutes the minimal functional substitutes of the antiangiogenic compounds of the suramin and suradista family. Particularly, 5-amino-2-naphthalenesulfonate (ANSA) has been identified from a wide window of charge, size, and relative position of substituent in the naphthalene ring as the derivative with the highest inhibitory activity.[8]

ANSA binds to the heparin-binding site of FGF in a defined orientation. Both the sulfonate and the amino groups set up hydrogen bonds, and the naphthalene ring establishes hydrophobic contacts with several aFGF residues implicated in the interaction of this protein with heparin.

Biomaterials researchers have demonstrated great interest on *macromolecular anticancer drugs* due to their success in the treatment of certain solid tumors.[9−11] In this sense, we have published recently the synthesis and characterization of two copolymeric systems based on *N*-vinylpyrrolidone (VP) or butyl acrylate (BA) and 2-acrylamido-2-methylpropane sulfonic acid (AMPS).[12] These systems inhibited fibroblast mitogenesis as a function of the content of the sulfonic group-bearing monomer (AMPS) and the microstructure of the obtained copolymers. Poly(BA-*co*-AMPS) copolymers (reactivity ratios: $r_{BA} = 3.68$; $r_{AMPS} = 0.30$) that presented AMPS rich sequences were more active than poly(VP-*co*-AMPS) based copolymers, and reactivity ratios ($r_{VP} = 0.12$; $r_{AMPS} = 0.27$) indicated the formation of an azeotropic system and a tendency to moderate alternating structures as both macroradicals preferably added the other monomer.

The aim of this study was the development of new antimitogenic heparinlike polysulfonated macromolecules based on a methacrylic derivative of 5-amine-2-naphthalenesulfonic acid (MANSA) to take advantage not only of the heparin like structure of these polysulfonated molecules, but also the advantages that polymeric materials present as drug delivery systems.

5-Amino-2-naphthalenesulfonic acid (ANSA) is a well characterized antimitogenic molecule that presents high activity.[8] ANSA was derived, including a reactive acrylic double bond in its structure, with the aim of getting, after polymerization, a pharmacologically active polymer, "polymer drug". MANSA was copolymerized with a hydrophilic monomer, *N*-vinylpirrolidone (VP), and a hydrophobic monomer, butylacrylate (BA), giving rise to two copolymeric systems with different microstructure, morphology, and antiangiogenic activity. This approach gives the opportunity to compare the relationship of the structure and morphology of the macromolecular systems with the corresponding bioactivity.

Materials and Methods

Reagents. 5-Amine-2-naphthalenesulfonic acid (ANSA, 97%) was provided by Avocado and used as received. *N*-Vinylpyrrolidone (VP, >99%) and butyl acrylate (BA, >99%), both from Sigma-Aldrich, were carefully distilled under reduced pressure. Dioxane (Panreac) was refluxed over potassium hydroxide (150 g/L) for 12 h and distilled under nitrogen. Dimethylsulfoxide (DMSO, Scharlau), *N*,*N*,*N*′,*N*′-tetramethylethylene diamine (TEMED, Acros), dimethylformamide (DMF, Sigma), dichloromethane (DCM, Fluka), methanol (Fluka), acetone (Carlo Erba), and lithium bromide (Sigma) were used without further purification. Azobis(isobutyronitrile) (AIBN, Merck) was recrystallized twice from ethanol. Methacryloylchloride (>97%, Fluka) and triethylamine (99.5%, Fluka) were distilled under nitrogen before used.

Synthesis of the ANSA-Containing Monomer. A methacrylic derivative of ANSA (MANSA) was prepared in two steps. First, the sodium salt of ANSA was obtained by the neutralization of ANSA (50 mmol in 100 mL) using a 0.9 M NaOH solution added dropwise until pH 8 was reached. The solution was filtered and the filtrate dried under vacuum. Second, the sodium salt of ANSA was reacted with methacryloyl chloride, at 0 °C, in the presence of triethylamine. The sodium salt of ANSA (0.02 M) and the triethylamine (0.02 M) were dissolved in DMF (50 mL). The methacryloyl chloride was added dropwise during at least 1 h under nitrogen flux at ice-bath temperature (Figure 1). The reaction was kept under magnetic stirring during 24 h. The precipitated triethylamine chloride was removed by filtration and DMF was evaporated under vacuum. The monomer was finally purified by column chromatography using dichloromethane−methanol (80:20) as mobile phase and Florisil 60/100 (magnesium−silica gel, Avocado) as solid phase. The yield of this process was 70%.

Synthesis of the Copolymers. Two different MANSA-based copolymeric systems were synthesized by free radical copolymerization (Table 1).

MANSA was copolymerized with VP or BA to obtain polymers with a different hydrophilic−hydrophobic balance. Poly(BA-*co*-MANSA) and poly(VP-*co*-MANSA) macromolecules were synthesized in water−dioxane (80:20). For each reaction, the appropriate monomers were mixed in suitable proportions to obtain a total monomer concentration of 0.5 M. The solution was deoxygenated bubbling pure nitrogen during 30 min. The polymerization reaction was induced thermally at 60 °C using AIBN (1.5×10^{-2} M) as free radical initiator (Figure 2). After 24 h, the polymer was precipitated in acetone and redissolved in water. The solution was then dialyzed (Slide-A-Lyser 3.5K Dialysis Cassette, 3500 molecular weight cutoff, PIERCE) against deionized water for 48 h to minimize the presence of residual unreacted monomers and low molecular weight molecules. Finally, all copolymers were isolated by freeze-drying.

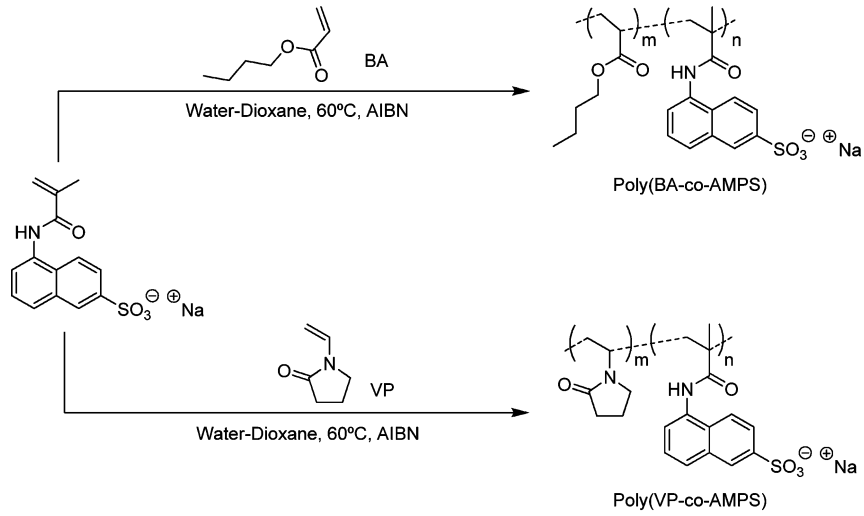

Figure 2. Copolymers synthesis.

Polymer Characterization. *NMR Analysis.* ^{1}H NMR and was performed in an INOVA-400 apparatus operating at 400 MHz and 333 K. The spectra were recorded using a 5% (w/v) D_2O (Merck) solution. Copolymer composition was calculated from ^{1}H NMR spectra.

Reactivity Ratios. The reactivity ratios (r_1 and r_2) of the comonomers were determined by nonlinear Tidwell−Mortimer and Levenberg−Marquardt methods.[13,14] Briefly, a series of low conversion copolymers (<10%) were prepared by free radical copolymerization in the same conditions as described in the previous section. At appropriate times, the reactions were stopped by pouring the solutions into acetone; the precipitate was dissolved in H_2O and freeze-dried before the determination of the feed and copolymer molar fractions by ^{1}H NMR characterization.

Particle Size Distribution and Zeta Potential. Particle size distribution and zeta potential of the nanoparticles were determined using a Zetasizer NanoZS (Malvern Instruments, U.K.) equipped with a HeNe laser beam with a wavelength of 633 nm and a scattering angle of 173°. The zeta potential measurements were performed in disposable folded capillary cells (DTS1060, Malvern Instruments) and particle-sized measurements in square polystyrene cuvettes (DTS0012, Malvern Instruments) with 0.25 mg/mL aqueous solutions, at 37 °C. All samples were filtered through 0.45 μm Millipore membrane prior to analysis.

Hydrodynamic diameter and polydispersity index were determined by dynamic light scattering (DLS). The intensity of light scattered was used to calculate the mean hydrodynamic diameter (*Z*-average mean), based on the Stokes−Einstein equation,[15] assuming the particle to be spherical. For each sample, the statistical mean and standard deviation of data were calculated from at least five measurements.

Zeta potential analysis was carried out using laser Doppler electrophoresis (LDE) with 30 runs per measurement. The zeta potentials were automatically calculated from the electrophoretic mobility using the Smoluchowski's approximation.[16] This approximation is generally applied when the measurements are carried out in aqueous media and considers that Henry's function takes a value of 3/2.

$$U_E = \frac{2\varepsilon z f(ka)}{3 \cdot \eta} \rightarrow z \approx U_E(\eta/\varepsilon)$$

where U_E = electrophoretical mobility, z = zeta potential, ε = dielectric constant, η = viscosity, and $f(ka)$ = Henry's function.

TEM Microscopy. Transmission electron microscopic (TEM) analysis was done on a Zeiss, EM10C instrument, operating at an acceleration voltage of 50 kV. An aqueous solution of the polymer (0.05% w/v) was mixed with uranil acetate (2% w/v) and mounted by casting in a PVA-coated Cu TEM grid. The sample was allowed to dry in ambient conditions.

TGA Experiments. A Perkin-Elmer TGA-7 interfaced to a thermal analysis data system TAC7/DX was used to study the thermal stability of the polymers. Thermograms were obtained under a nitrogen atmosphere, between 40 and 550 °C, using a constant heating rate of 10 °C/min.

GPC Experiments. Number and weight average molecular weight and polydispersity of all the specimens were obtained by gel permeation chromatography (GPC), using a Perkin-Elmer Series 200 coupled to a UV/vis detector (278 nm). The system was formed by three Resipore Varian columns of 1000, 500, and 100 Å nominal pore diameter (Polymer Laboratories). By flowing a degassed mobile phase, 0.1% lithium bromide in DMF, at 1 mL/min, a GPC diagram was obtained as a function of the elution time. The molecular weight was determined based on the calibration curve obtained from monodisperse polystyrene standard samples with molecular weights between 580 and 370000 g/mol (Polymer Laboratories). Data were analyzed using the Perkin-Elmer TurboSec program.

Analysis of the Bioactivity. The effect of the synthesized polymers on aFGF-driven mitogenesis and quiescent viability of fibroblasts was studied in vitro as previously described by Fernández Tornero et al.[8] Briefly, Balb/c 3T3 fibroblasts were seeded in 96-well plates at a density of 9000 cells/mL (1800 cells/well) using Dulbecco's modified Eagle's medium (DMEM), supplemented with 10% calf serum as culture medium and incubated during 6 h. The medium was replaced with DMEM/Ham's F-12 (100 μL/well) and incubated at 37 °C and 5% CO_2. After 14 h, aFGF (6.40 ng/mL), 3 KDa heparin (100 μg/mL), and the polymer (in concentrations between 0 and 10 mg/mL) were added to 0.1% BSA in DMEM and 10 μL of the solutions was added to the wells and incubated during 72 h. To fix the cells, 10 μL of glutaraldehyde (25%) was added to all wells, and the plate was incubated for 10 min before washing with milli-Q water and drying at 37 °C. Fixed cells were dyed using a crystal violet solution (1 mg/mL) in 50 mM phosphate buffer pH 7.2. The solution was removed after 10 min incubation and cells were washed to remove the dye excess before drying at 37 °C. Finally, 10% acetic acid (100 μL) was added, the solution was mixed, and differential absorbance (A620 nm-A690 nm) was measured on a Synergi HT Multi-Detection Microplate Reader (Biotek).

Cell viability was evaluated in the presence of the synthetic polymers, as described above, however, aFGF was not added to the culture medium.

Table 2. Composition and Molecular Weight of the Synthesized Poly(VP-*co*-MANSA) Obtained by ^{1}H NMR and GPC

	composition				GPC		
	$F(VP)_{feed}$	$f(VP)_{copol}$	$w(VP)_{copol}$	yield (%)	M_w	M_n	M_w/M_n
poly(VP-*co*-MANSA) (50:50)	50	73	50	22.8	11100	8500	1.30
poly(VP-*co*-MANSA) (60:40)	60	85	68	19.1	11900	8800	1.35
poly(VP-*co*-MANSA) (80:20)	80	90	77	40.6	27200	22800	1.19

Results and Discussion

Two different copolymeric families based on the synthesized monomer, MANSA, were obtained by free radical copolymerization (Tables 1 and 2). MANSA was reacted with VP (hydrophilic) or BA (hydrophobic) to obtain macromolecules with different hydrophilic−hydrophobic balance. The reactions including MANSA presented a limited conversion due to the low reactivity of this monomer and the contribution of the conjugated sulfonic groups with the naphthalene aromatic ring.

Independent of the initial feed composition, the free radical copolymerization of BA and MANSA gave rise to copolymers with rather similar comonomeric compositions. The polydispersity index for these copolymers was relatively low for this polymerization mechanism (free radical polymerization). This can be due to the relative stabilization of the macroradicals when MANSA is incorporated into the chains, due to the electrons delocalization by conjugation of the methacrylic moiety with the high electron density of naphthalene aromatic ring. Molecular weight of all the poly(BA-*co*-MANSA) copolymers was low (Table 1) and increased as the MANSA concentration decreased. As a consequence of the relatively high stabilization of growing free radicals, the molecular weight of the copolymers obtained was moderately low considering a free radical polymerization mechanism. Moreover, the polydispersity index in most of the compositions studied is near to the unity, which is characteristic of the controlled free radical polymerization with specific transfer agents, as described by Rizzardo et al.[17−19] for the reversible addition−fragmentation chain transfer (RAFT) polymerization. The high ionizable character and complexing interactions of the conjugated sulfonic group with the naphthalene ring and the methacrylic counterpart seems to dominate and modulate the polymerization steps, that is, propagation−stabilization of the free radicals or even the termination step, in such a way that the copolymers generated present a very homogeneous molecular weight distribution. The limiting conversion affects to the incorporation of the less reactive species, MANSA, and therefore, this is the reason for the big difference between the experimental average composition of copolymers and the concentration of monomers in the initial feed (Table 1).

The copolymerization of VP and MANSA proceeded in a similar way as the system described before. The obtained copolymer composition varied as a function of MANSA feed molar concentration (Table 2). Polydispersity index of these copolymers was also very low. Molecular weight of all the poly(VP-*co*-MANSA) copolymers was low and increased as the MANSA concentration decreased. It is well-known that the pyrrolidone group is a potent complexing agent for ionic groups including cations (calcium, magnesium, copper, tin, etc.) and also a recognized solvating group. Therefore, it is not surprising to find a relatively strong control of the polymerization reaction through the direct interactions of the *N*-vinylpyrrolidone or the growing chains ending in *N*-vinylpyrrolidone units with the conjugated sulfonic groups, although these are ionized as sodium salts. The consequence is a strict control of the molecular weight and molecular weight distribution, giving polydispersity indexes close to the unity instead of a random free radical polymerization that would give a polydispersity index around 2.5 or even higher.

Polymer Characterization. *NMR Experiments.* Copolymer molar composition of all polymers was determined by ^{1}H NMR analysis (Tables 1 and 2). Absence of acrylic proton signals (Figure 3) confirmed the elimination of any residual monomer after the dialysis process.

The BA and MANSA mole fractions of the copolymer were calculated using the integrated peak intensities according to the following equations:

$$[BA] = (I_{18}/2)/(I_{18}/2) + (I_{6,7,8,10,12,13}/6)$$

$$[MANSA] = (I_{6,7,8,10,12,13}/6)/(I_{18}/2) + (I_{6,7,8,10,12,13}/6)$$

The VP and MANSA mole fractions of the copolymer were calculated by

$$[VP] = (I_{15,16,20}/5)/(I_{15,16,20}/5) + (I_{6,7,8,10,12,13}/6)$$

$$[MANSA] = (I_{6,7,8,10,12,13}/6)/(I_{15,16,20}/5) + (I_{6,7,8,10,12,13}/6)$$

Reactivity Ratios. Reactivity ratios are two kinetic parameters that give a clear idea of the average composition and the monomer sequence distribution in statistical copolymer systems (Table 3).

Poly(BA-co-MANSA) System. The poly(BA-*co*-MANSA) system presented values of $r_{BA} = 14.71$ and $r_{MANSA} = 0.26$. Both propagating species preferably added BA that presented a much higher reactivity than MANSA. Consequently, there was a tendency toward the formation of long sequences or blocks of the polymerizing species as a consequence of the preferential addition of BA units to the free radical growing chains. At the beginning of the reaction, BA-rich sequences were formed until it was almost consumed; MANSA-rich sequences or blocks were subsequently formed, as predicted in Figure 4, where the evolution of the instantaneous copolymer molar fraction as a function of conversion and feed molar fraction is represented using the calculated reactivity ratios. However, copolymerization reactions did not reach total conversion and MANSA did not form long sequences. Only a few MANSA units were incorporated at the end of the macromolecules before the reaction stopped. The incorporation of this amount of MANSA monomer was enough to give rise to the formation of micelles in aqueous medium, even though BA is a highly hydrophobic component.

Poly(VP-co-MANSA) System. The poly(VP-*co*-MANSA) system presented values of $r_{VP} = 13.40$ and $r_{MANSA} = 0.12$. As in the previous system, there was a tendency toward sequential addition of the two monomers due to both propagating species preferably added VP. The most reactive monomer (VP) tended to form long VP sequences or blocks until it was consumed; MANSA subsequently formed long sequences or blocks (Figure 5). However, as mentioned in the previous system, copolym-

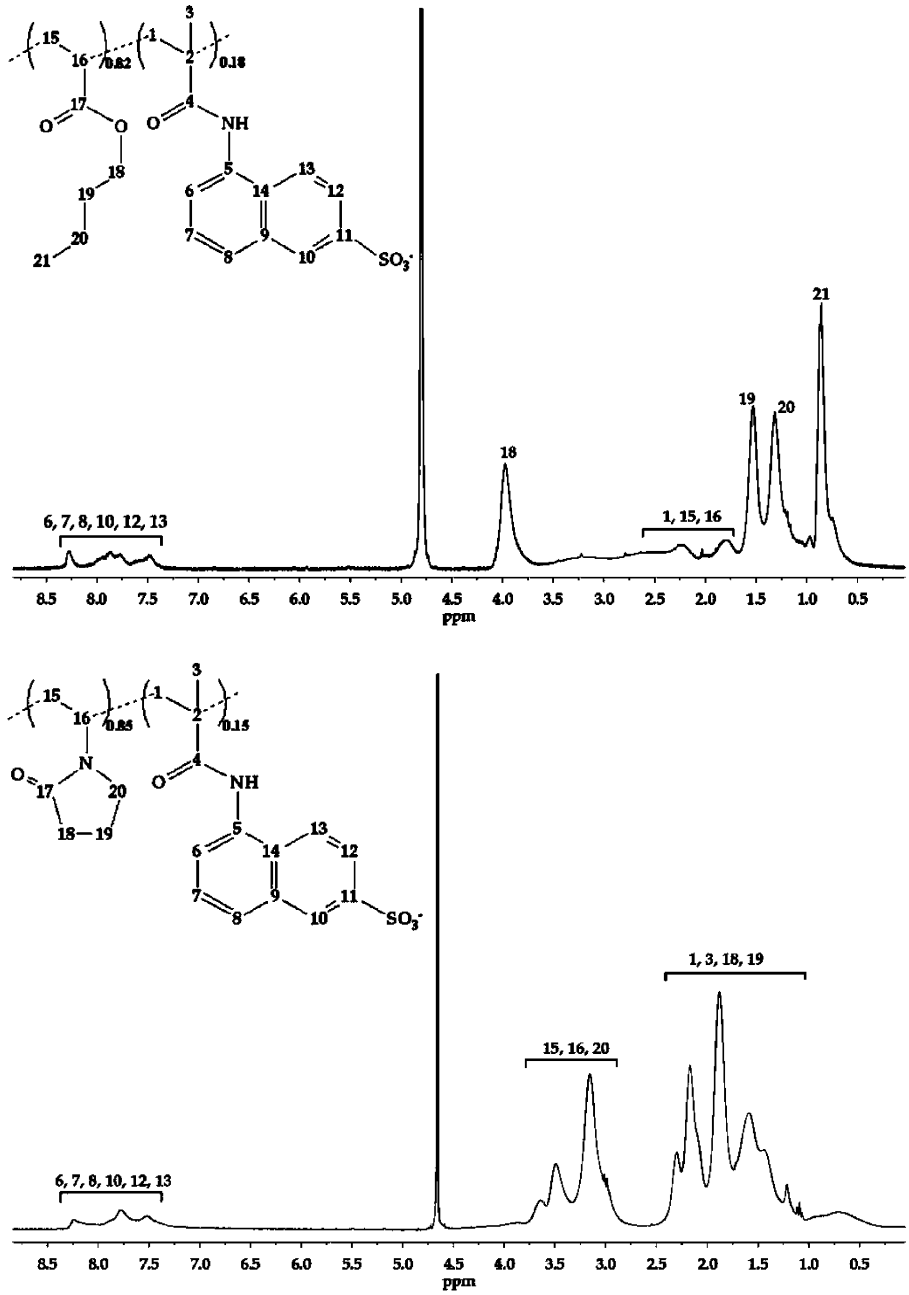

Figure 3. ^{1}H NMR spectra of a poly(BA-*co*-MANSA) and a poly(VP-*co*-MANSA).

Table 3. Reactivity Ratios of the Copolymeric Systems Determined by In Situ ^{1}H NMR

	reactivity ratios	
poly(BA-*co*-MANSA)	$r_{BA} = 14.71$	$r_{MANSA} = 0.26$
poly(VP-*co*-MANSA)	$r_{VP} = 13.40$	$r_{MANSA} = 0.12$

erization reactions did not proceed until total conversion and MANSA did not form long sequences, but only one or two MANSA units were incorporated at the end of the macromolecules before the reaction stopped.

The calculated reactivity ratios and the relative low yield of the reactions indicated a similar behavior toward chain copolymerization for the two copolymeric systems. Both systems presented a similar monomer distribution in the copolymeric chains, however, the different hydrophilicity of the comonomers (hydrophilic VP, or hydrophobic BA) determined different segments or chains conformations. The distribution of those sequences give a clear supramolecular organization of the synthesized polymer systems, with a significant effect on the antiproliferative activity, as will be demonstrated in the following sections.

Particle Size Distribution, TEM, and Zeta Potential. The free radical copolymerization of BA and MANSA gave rise to poly(BA-*co*-MANSA) copolymers with a particular distribution of the monomers. As described before, long BA-rich chains (very hydrophobic) were formed at the beginning of the reaction and one or two MANSA units (very hydrophilic) were incorporated at the end of the macromolecule before the copolymerization reaction stopped. The combination of these hydrophobic and hydrophilic moieties and the rather homogeneous molecular weight distribution of the macromolecules favor the self-assembling of the macromolecules in contact with water due to the hydrophobic effect.[20] The hydrodynamic diameter of self-assembled nanoparticles ranged between 20 and 100 nm (Table 4), indicating the formation of micelles.[21] According to the results quoted in Table 4, seems to be logical that the

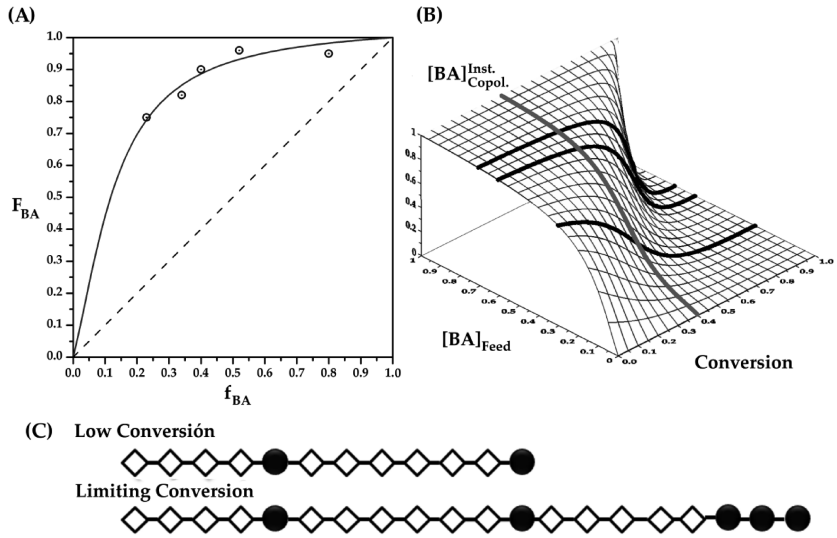

Figure 4. (A) Composition diagram for the system poly(BA-*co*-MANSA); low conversion experimental reactions (circles). (B) Instantaneous BA copolymer molar fraction for the system poly(BA-*co*-MANSA) as a function of conversion and BA feed molar fraction. The thick solid black lines represent the course of the reactions to obtain the synthesized copolymers ($F(BA)_{feed} = 0.30; 0.60; 0.70$) and the thick solid gray line represent the *limiting conversion*. (C) Monomer distribution scheme of a reaction: solid circles, MANSA; empty diamonds, BA.

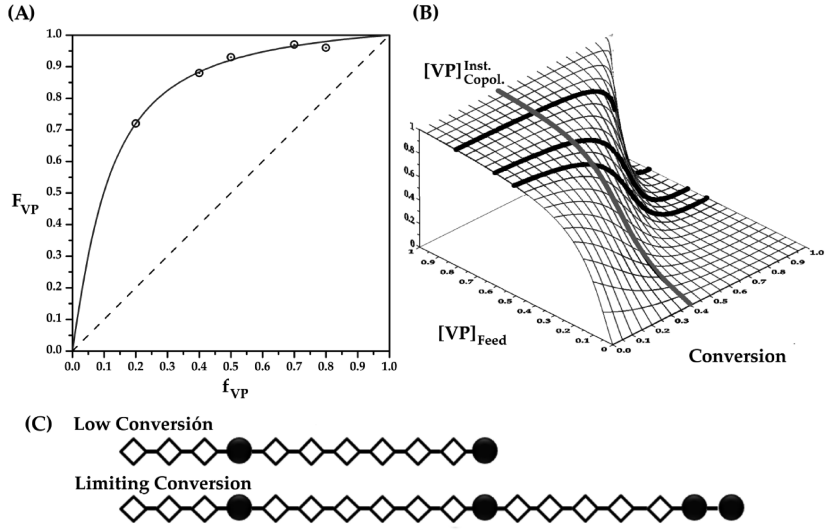

Figure 5. (A) Composition diagram for the system poly(VP-*co*-MANSA); low conversion experimental reactions (circles). (B) Instantaneous VP copolymer molar fraction for the system poly(VP-*co*-MANSA) as a function of conversion and VP feed molar fraction. The thick solid black lines represent the course of the reactions to obtain the synthesized copolymers ($F(VP)_{feed} = 0.50; 0.60; 0.80$) and the thick solid gray line represent the limiting conversion. (C) Monomer distribution scheme of a reaction: solid circles, MANSA; empty diamonds, VP.

Table 4. Hydrodynamic Diameter and Zeta Potential Measured by Dynamic Light Scattering and Electrophoretic Mobility

	hydrodynamic diameter (nm)	polydispersity index	zeta potential (mV)
poly(BA-*co*-MANSA) (30:70)	21.7 ± 0.1	0.357 ± 0.005	−55.6 ± 3.61
poly(BA-*co*-MANSA) (60:40)	41.5 ± 0.5	0.559 ± 0.097	−43.4 ± 9.85
poly(BA-*co*-MANSA) (70:30)	97.3 ± 0.2	0.274 ± 0.080	−29.3 ± 5.81

micellar nanoparticles correspond to the supramolecular assembly of an increase number of macromolecules. If we consider the average size of the macromolecular chains, according to the molecular weight (Tables 1 and 2), unimacromolecular micelles should give a much lower size that the observed by light scattering (Table 4).

The TEM micrograph (Figure 6) shows the view of nanoparticles in the form of packed micelles that are formed when poly(BA-*co*-MANSA) are put in contact with water, as it happens with other amphiphilic polymer systems like poly(ethylene oxide-*co*-butylene oxide) block copolymers.[22,23] The average size ranged between 5−10 nm.

The formation of charged self-assembled nanostructures was analyzed by the measurement of the zeta potential of the micelles in water dispersions. The formation of a net charge at the particle surface affects the distribution of ions in the surrounding interfacial region. The electrical potential decrease with the distance to the particle and two regions can be differentiated: an inner region (Stern layer) with the ions strongly bounded and an outer layer (diffuse layer).[24] Between these two regions exists a boundary where the ions and particles form a stable entity. The potential at this point is easy to measure and is the zeta potential. The negative measured values indicated that the sulfonic groups from MANSA units were located on the surface of the micelles forming a hydrophilic electrostatic shell, and BA-rich segments were located inside the particles forming a hydrophobic BA-core (Figure 7).

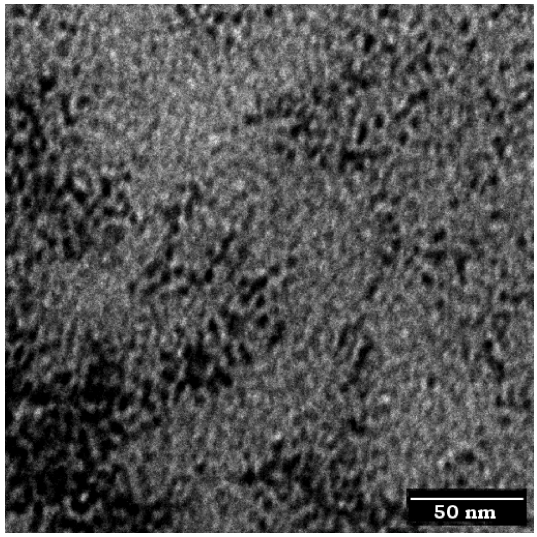

Figure 6. TEM image of the packed micelles formed from self-assembly of poly(BA-*co*-MANSA) (60:40) in aqueous solution at room temperature.

The magnitude of the zeta potential gives an indication of the stability of the micelles. Zeta potential of poly(BA-*co*-MANSA) containing 18 or 20 molar % of MANSA units was lower than −30 mV (Table 4), and therefore, the supramolecular structures formed were considered stable.[25] The *z*-potential for the copolymer with a content in MANSA of 11% indicates that there is a critical concentration of the ionized monomer for the formation of stable nanoparticles that may be around 10−12% of MANSA in the copolymer chains.

The formation of self-assembled structures was not detected when poly(VP-*co*-MANSA) macromolecules were dissolved in water.

TGA Experiments. Poly(BA-co-MANSA) System. Figure 8 demonstrates that poly(BA) chains decompose in a single weight loss step to give oligomeric hydrocarbon compounds at temperatures ranging from 300 to 450 °C, with a temperature of a maximum decomposition rate at 410 °C. The TGA curve for poly(MANSA) showed also a single weight loss stage with a temperature of a maximum decomposition rate at 300 °C, probably due to the radical decomposition of the macromolecular chains. Heating of poly(BA-*co*-MANSA) copolymers is accompanied by a gradual mass loss from 50 to 150 °C following a plateau extending to 200−250 °C, depending on the specific sample. This mass loss can be related to the release of water adsorbed by the samples. Degradation occurred above 250 °C as it is typical for acrylic polymers, to give a residue that corresponds to the sulfate sodium salt and carbonaceous species, which are stable up to at least 550 °C in N_2 atmosphere. The amount of residue is coherent with the composition of the copolymer analyzed.

Poly(VP-co-MANSA) System. Poly(VP) degradation occurred between 350−470 °C, with a temperature of maximum decomposition rate of 440 °C. Poly(VP) chains decompose by the action of temperature by the random cleavage of the main chains to give rise to hydrocarbon compounds of low molecular weight.

As in the previous system, heating of poly(VP-*co*-MANSA) copolymers is accompanied by a gradual mass loss from 50 to 150 °C, followed by a plateau extending to 250−325 °C, depending on the specific sample. This mass loss was related to the release of water adsorbed by these hydrophilic samples. Further heating leads to a two-stage process that could correspond to the decomposition of VP-MANSA sequences (from 300 to 360 °C); the second phase (from 360 to 460 °C) corresponds to the degradation of VP-rich sequences (Figure 9).

A comparison of the thermograms drawn in Figures 8 and 9 makes clear the significant difference of the effect of MANSA sequences in both copolymer systems. The thermal stability of the series poly(BA-*co*-MANSA), considered as the initial temperature of the thermal degradation process, decreases noticeably by the introduction of MANSA sequences, whereas in the series poly(VP-*co*-MANSA) the effect is less significant. This is a consequence of the different morphologies of both copolymer systems and the self-assembled structures of the system poly(BA-*co*-MANSA) in comparison with the more hydrophilic and logically homogeneous conformational arrangement of the poly(VP-*co*-MANSA) copolymers.

Analysis of Bioactivity. FGF is potentially a key target for developing antitumoral therapies based on antiangiogenesis because it has been associated with tumor vascularity and, therefore, with tumor malignancy.[10] Spivak-Kroizman et al. stated that the interaction between HSPGs/FGF/FGFR is strictly necessary to trigger the proangiogenic signal.[26] Therefore, the synthetic molecules that attach to the HSPGs binding site of the FGF may act as angiogenic inhibitors, as they hamper the coupling between FGF and HSPGs, avoiding the interaction and activation of the FGFR with tyrosine kinase activity.

Between all the FGF isoforms, aFGF is a unique system to explore the molecular basis of new polysulfonated macromolecules, because it is less stable than basic FGF (bFGF) in the absence of polyanions and requires the presence of a molecule like heparin for significant biological activity. Moreover, aFGF presents low specificity and can complex with a number of sulfonated molecules.

The effect of the MANSA-containing macromolecules on the mitogenic activity of Balb/c 3T3 fibroblasts induced by one of the most relevant pro-angiogenic growth factors, aFGF, was investigated as a step to evaluate the bioactivity of these polymers. Fibroblasts were used in the experiments due to the high sensitivity of these cells to the aFGF activity.

Poly(BA-co-MANSA) System. Figure 10 summarizes the mitogenesis assay performed to elucidate the biological activity of this copolymeric system. In the presence of aFGF, the mitogenic effect ascribed to the addition of the growth factor was clearly compensated and, at the end, inhibited by all the assayed copolymers as a function of the copolymer concentration in the medium. The three copolymers were active at all the assay concentrations, and interestingly, the copolymer that incorporated the highest concentration of MANSA monomer, poly(BA-*co*-MANSA) (30:70), presented the highest antimitogenic activity. This was attributed to the formation of supramolecular structures due to the hydrophilic/hydrophobic domains formed during the copolymerization reaction. This copolymeric system formed charged nanoparticles as described in the previous section. These nanoparticles presented different surface charge as demonstrated by the *z*-potential values (Table 3) related to the MANSA concentration on the surface.

Poly(BA-*co*-MANSA) copolymers had no effect on cells that did not receive aFGF (Figure 10). It is important to stress that the absence of floating cells or other signs of lysis indicated that these polymers were not toxic to the cells.

Poly(VP-co-MANSA) System. Figure 11 summarizes the proliferation assay results obtained for this family of copolymers. Poly(VP-*co*-MANSA) copolymers were less active than poly(BA-*co*-MANSA) copolymers because they did not present activity when added at low concentrations. Poly(VP-*co*-

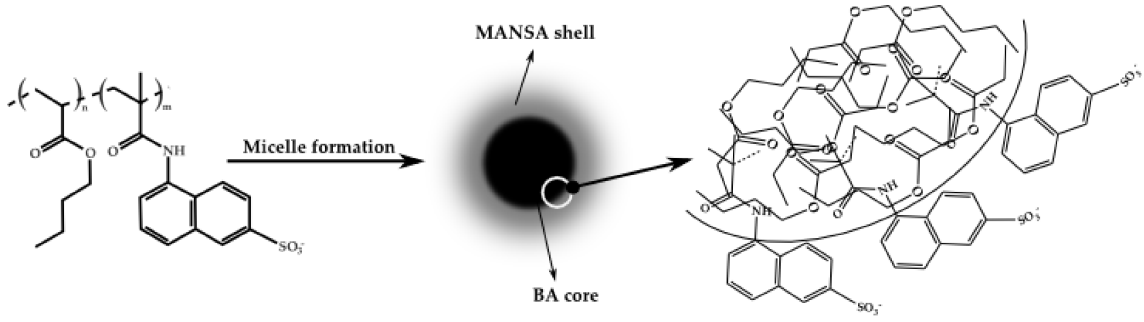

Figure 7. Formation of poly(BA-*co*-MANSA) micelles in water.

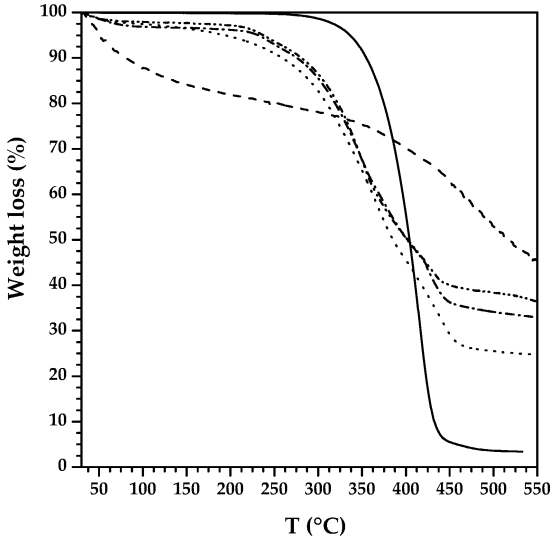

Figure 8. Thermal degradation of poly(BA-*co*-MANSA); solid line, poly(BA); dot line, poly(BA-*co*-MANSA) (70:30); dash-dot line, poly(BA-*co*-MANSA) (60:40); dashed-dot-dot line, poly(BA-*co*-MANSA) (30:70); dashed line, poly(MANSA).

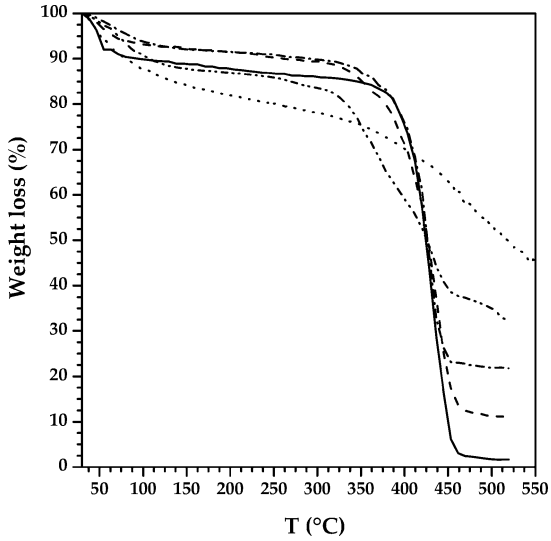

Figure 9. Thermal degradation of poly(VP-*co*-MANSA) copolymers; solid line, poly(VP); dashed line, poly(VP-*co*-MANSA) (60:40); dash-dot, poly(VP-*co*-MANSA) (50:50); dash-dot-dot, poly(VP-*co*-MANSA) (40:60); dot line, poly(MANSA).

MANSA) (80:20) and poly(VP-*co*-MANSA) (60:40) did not have a clear inhibitory effect on cell mitogenesis until 250 μg/mL of polymer was added to the culture medium. And poly(VP-*co*-MANSA) (50:50), the copolymer that incorporated the highest amount of MANSA, presented activity only at concentrations higher than 75 μg/mL.

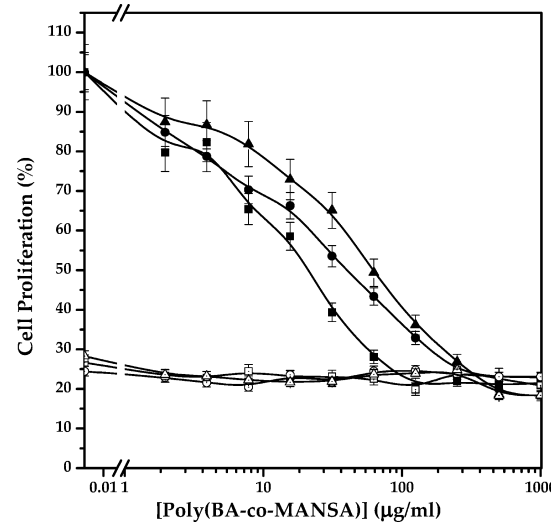

Figure 10. Effect of the poly(BA-*co*-MANSA) copolymers on Balb/c-3T3 fibroblast proliferation: solid symbols, aFGF-induced proliferation activated by heparin; empty symbols, toxicity control, no aFGF was added; square, poly(BA-*co*-MANSA) (30:70); triangle, poly(BA-*co*-MANSA) (60:40); circle, poly(BA-*co*-MANSA) (70:30).

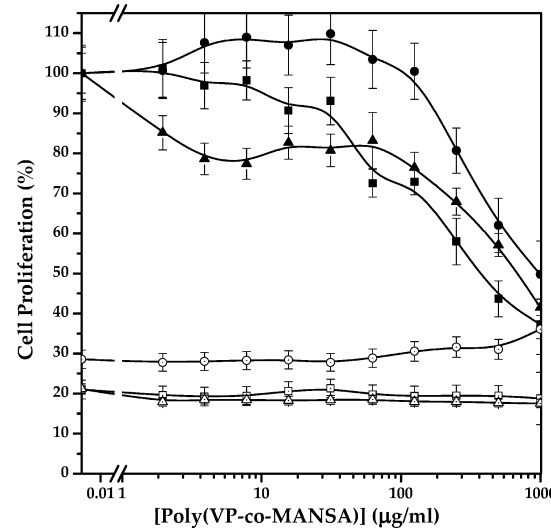

Figure 11. Effect of the poly(VP-*co*-MANSA) copolymers on Balb/c-3T3 fibroblast proliferation: solid symbols, aFGF-induced proliferation activated by heparin; empty symbols, toxicity control, no aFGF was added; square, poly(VP-*co*-MANSA) (50:50); triangle, poly(VP-*co*-MANSA) (60:40); circle, poly(VP-*co*-MANSA) (80:20).

Poly(VP-*co*-MANSA) copolymers did not develop an effect on cells that did not receive aFGF (Figure 11). Additionally, the absence of floating cells or other signs of lysis indicated that these polymers were not toxic to the cells.

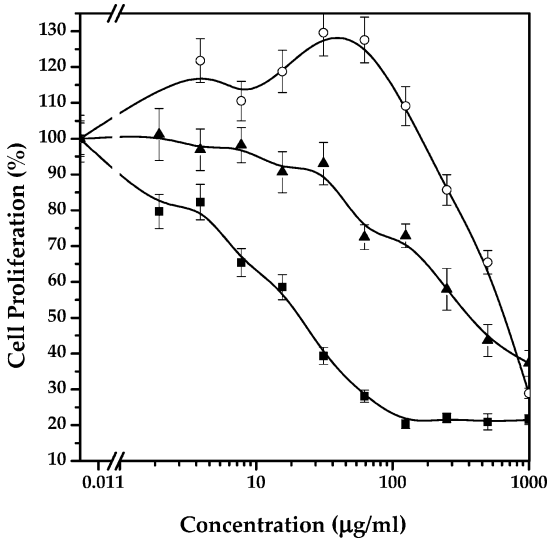

Figure 12. Effect of the poly(BA-*co*-MANSA) (solid square), poly(VP-*co*-MANSA) (solid triangle), and poly(BA-*co*-AMPS) (empty circles) with molar compositions in the copolymer of 20% MANSA, 27% MANSA, and 27% AMPS, respectively, on Balb/c-3T3 fibroblast proliferation.

A comparison of the inhibitory effect of cell proliferation of the poly(BA-*co*-MANSA) system with poly(VP-*co*-MANSA) systems shows that the morphology of the bioactive micelles of poly(BA-*co*-MANSA) provides an optimal orientation of the sulfonic acid for the interaction with the growth factor. This gives an increasing inhibitory bioactivity of the poly(BA-*co*-MANSA) with the concentration at very low values, whereas, in the case of poly(VP-*co*-MANSA), the activity is observed at higher concentrations of the copolymeric system (Figure 12). All these results suggest that the organization of these macromolecules in supramolecular structures can change the active monomer availability and its activity.

A comparison of the inhibitory effect of cell proliferation of the poly(BA-*co*-MANSA) system with another rather similar system based on copolymers of 2-acrylamido-2-methylpropane sulfonic acid, poly(BA-*co*-AMPS), described in a recent publication,[12] also shows that the type of interaction between the active group and the FGF influences the biological activity. This gives an increasing inhibitory bioactivity of the poly(BA-*co*-MANSA) with the concentration at very low values, whereas, in the case of poly(BA-*co*-AMPS), the activity is observed at higher concentrations of the copolymeric system. This is clearly observed in Figure 12, where the cell proliferation values of the three copolymer systems with a rather similar composition of the bioactive component, MANSA or AMPS, are represented.

All these results demonstrate the great importance and influence of the microstructure and morphology of macromolecular systems in the bioactivity, which it is very frequently shown by natural bioactive macromolecular systems, such as proteins, hormones, growth factors, polysaccharides, and so on, and it is also well demonstrated by the comparison of the results obtained by the three polymer systems poly(BA-*co*-MANSA), poly(BA-*co*-AMPS), and poly(VP-*co*-MANSA).

Conclusions

New low toxicity bioactive and resorbable polymers with high antimitogenic activity have been prepared by a controlled free radical mechanism. The election of vinyl and acrylic monomers of different hydrophilic character in combination with the active sulfonated monomer gives rise to interesting copolymers which present a self-organizing nanoparticles with specific bioactivity through the complexation of active sulfonate groups of MANSA with aFGF.

The effect of the acrylic derivative of 5-amino-2-naphthalenesulfonic acid, MANSA, in free radical copolymerization reactions with BA or VP provides an excellent route for the preparation of controlled bioactive and resorbable polymer systems with interesting applications in the control of angiogenesis and tumoral processes.

Poly(BA-*co*-MANSA) amphiphilic copolymers form an interesting micellar morphology by self-assembling. The hydrophobic BA sequences are concentrated in the core of the nanoparticles and the hydrophilic MANSA units are located on the surface or shell of the nanoparticles. This property can be considered for the preparation of targeting bioactive nanoparticles by the encapsulation of hydrophobic molecules used as chemotherapeutic agents (taxotere, simvastatin, doxorubicin, etc.) that will be released in a controlled and modulated way in the site of action.

Acknowledgment. Partial financial support from MAT2007-63355 and "Ramon y Cajal Program" is gratefully acknowledged. Support from NoE EXPERTISSUES from the EC is also acknowledged. Authors thank the technical help provided by Marta Rodriguez from the UAH and Ainara Imaz from the EHU in the TEM experiments and the Zetasizer experiments, respectively.

References and Notes

(1) Quesada, A. R.; Oz, C.; Medina, M. A. Anti-angiogenic drugs: From bench to clinical trials. *Med. Res. Rev.* **2006**, *26* (4), 483–530.
(2) Zhong, H.; Bowen, J. P. Antiangiogenesis drug design: Multiple pathways targeting tumor vasculature. *Curr. Med. Chem.* **2006**, *13* (8), 849–862.
(3) Wheatley-Price, P.; Shepherd, F. A. Targeting angiogenesis in the treatment of lung cancer. *J. Thorac. Oncol.* **2008**, *3* (10), 1173–1184.
(4) Petersen, I. Antiangiogenesis, anti-VEGF(R) and outlook. In *Targeted Therapies in Cancer*; Dietel, M., Ed.; Springer: Berlin., 2007; pp 189−199.
(5) Auguste, P.; Javerzat, S.; Bikfalvi, A. Regulation of vascular development by fibroblast growth factors. *Cell Tissue Res.* **2003**, *314* (1), 157–166.
(6) Kathir, K. M.; Kumar, T. K. S.; Yu, C. Understanding the mechanism of the antimitogenic activity of suramin. *Biochemistry* **2006**, *45* (3), 899–906.
(7) Schneider, G. P.; Salcedo, R.; Dong, H. F.; Kleinman, H. K.; Oppenheim, J. J.; Howard, O. M. Z. Suradista NSC 651016 inhibits the angiogenic activity of CXCL12-stromal cell-derived factor 1Î±. *Clin. Cancer Res.* **2002**, *8* (12), 3955–3960.
(8) Fernández-Tornero, C.; Lozano, R. M.; Redondo-Horcajo, M.; Gómez, A. M.; López, J. C.; Quesada, E.; Uriel, C.; Valverde, S.; Cuevas, P.; Romero, A.; Giménez-Gallego, G. Leads for development of new naphthalenesulfonate derivatives with enhanced antiangiogenic activity. Crystal structure of acidic fibroblast growth factor in complex with 5-amino-2-naphthalenesulfonate. *J. Biol. Chem.* **2003**, *278* (24), 21774–21781.
(9) Satchi-Fainaro, R.; Duncan, R.; Barnes, C. M. *Polymer Therapeutics for Cancer: Current Status and Future Challenges*; Springer: Berlin, 2006; pp 1−65.
(10) Vicent, M. J.; Duncan, R. Polymer conjugates: Nanosized medicines for treating cancer. *Trends Biotechnol.* **2006**, *24* (1), 39–47.
(11) Duncan, R. Polymer conjugates for tumour targeting and intracytoplasmic delivery. The EPR effect as a common gateway. *Pharm. Sci. Technol. Today* **1999**, *2* (11), 441–449.
(12) Garciía-Fernaíndez, L.; Aguilar, M. R.; Fernaíndez, M. M.; Lozano, R. M.; Gimeínez, G.; Romaín, J. S. Antimitogenic polymer drugs based on AMPS: Monomer distribution−bioactivity relationship of water-soluble macromolecules. *Biomacromolecules* 2010.
(13) Tidwell, P. W.; Mortimer, G. A. An improved method of calculating copolymerization rectivity ratios. *J. Polym. Sci., Part A: Polym. Chem.* **1965**, *3*, 369–387.

(14) More, J. J. *Levenberg−Marquardt algorithm: implementation and theory*; Springer: Berlin, 1977.
(15) Kätzel, U.; Bedrich, R.; Stintz, M.; Ketzmerick, R.; Gottschalk-Gaudig, T.; Barthel, H. Dynamic Light Scattering for the Characterization of Polydisperse Fractal Systems: I. Simulation of the Diffusional Behavior. *Part. Part. Syst. Charact.* **2008**, *25* (1), 9–18.
(16) Hunter, R. J. *Foundations of colloid science*; Oxford University Press: Oxford, New York, 2001.
(17) Moad, G.; Chong, Y. K.; Skidmore, M. A.; Rizzardo, E.; Thang, S. H. *Advances in raft polymerization: Improved nanostructured materials*, 1st ed.; American Chemical Society, Polymer Preprints, Division of Polymer Chemistry: New Orleans, LA, 2008; pp 293−294.
(18) Moad, G.; Rizzardo, E.; Thang, S. H. Toward living radical polymerization. *Acc. Chem. Res.* **2008**, *41* (9), 1133–1142.
(19) Moad, G.; Rizzardo, E.; Thang, S. H. Living radical polymerization by the RAFT process: A second update. *Aust. J. Chem.* **2009**, *62* (11), 1402–1472.
(20) Tanford, C. Interfacial free energy and the hydrophobic effect. *Proc. Natl. Acad. Sci. U.S.A.* **1979**, *76* (9), 4175–4176.
(21) Blanazs, A.; Armes, S. P.; Ryan, A. J. Self-assembled block copolymer aggregates: From micelles to vesicles and their biological applications. *Macromol. Rapid Commun.* **2009**, *30* (4−5), 267–277.
(22) LoPresti, C.; Lomas, H.; Massignani, M.; Smart, T.; Battaglia, G. Polymersomes: Nature inspired nanometer sized compartments. *J. Mater. Chem.* **2009**, *19* (22), 3576–3590.
(23) Battaglia, G.; Ryan, A. J. Effect of amphiphile size on the transformation from a lyotropic gel to a vesicular dispersion. *Macromolecules* **2005**, *39* (2), 798–805.
(24) Chiriac, A. P.; Nita, L. E.; Neamtu, I.; Bercea, M. Contribution to polymer nanoparticles analysis by laser light scattering. *Polym. Test.* **2009**, *28* (8), 886–890.
(25) Sun, Z.; Xu, S.; Dai, G.; Li, Y.; Lou, L.; Liu, Q.; Zhu, R. A microscopic approach to studying colloidal stability. *J. Chem. Phys.* **2003**, *119* (4), 2399–2405.
(26) Spivak-Kroizman, T.; Lemmon, M. A.; Dikic, I.; Ladbury, J. E.; Pinchasi, D.; Huang, J.; Jaye, M.; Crumley, G.; Schlessinger, J.; Lax, I. Heparin-induced oligomerization of FGF molecules is responsible for FGF receptor dimerization, activation, and cell proliferation. *Cell* **1994**, *79* (6), 1015–1024.

BM100223D